

Article

# Analysis on the Fire Growth Rate Index Considering of Scale Factor, Volume Fraction, and Ignition Heat Source for Polyethylene Foam Pipe Insulation

Jung Wook Park <sup>1</sup>, Ohk Kun Lim <sup>2</sup> and Woo Jun You <sup>1,\*</sup>

<sup>1</sup> Department of Architecture & Fire Safety, Dong Yang University, Yeongju 36040, Korea; kkisd0123@naver.com

<sup>2</sup> R&D Laboratory, Korea Fire Institute, Yongin 17088, Korea; terence@kfi.or.kr

\* Correspondence: wjyou@dyu.ac.kr; Tel.: +82-54-630-1297

Received: 17 June 2020; Accepted: 2 July 2020; Published: 15 July 2020



**Abstract:** The fire growth rate index (*FIGRA*), which is the ratio of the maximum value of the heat release rate ( $Q_{max}$ ) and the time ( $t_{max}$ ) to reach the maximum heat release rate, is a general method to evaluate a material in the fire-retardant performance in fire technology. The object of this study aims to predict *FIGRA* of the polyethylene foam pipe insulation in accordance with the scale factor ( $S_f$ ), the volume fraction of the pipe insulation ( $VF$ ) and the ignition heat source ( $Q_{ig}$ ). The compartments made of fireboard have been mock-up with 1/3, 1/4, and 1/5 reduced scales of the compartment as specified in ISO 20632. The heat release rate data of the pipe insulation with the variation of  $S_f$ ,  $VF$ , and  $Q_{ig}$  are measured from 33 experiments to correlate with *FIGRA*. Based on a critical analysis of the heat transfer phenomenon from previous research literature, the predictions of  $Q_{max}$  and  $t_{max}$  are presented. It is noticeable that the fire-retardant grade of the polyethylene foam pipe insulation could have Grade B, C, and D in accordance with the test conditions within  $\pm 15\%$  deviation of the predicted *FIGRA*. In case of establishing the database of various types of insulation, the prediction models could apply to evaluate the fire-retardant performance.

**Keywords:** pipe insulation; fire growth rate index; scale factor; volume fraction; ignition heat source; maximum heat release rate; time to reach maximum HRR (heat release rate)

## 1. Introduction

Insulation is widely used in buildings as an important material to prevent energy loss of architecture [1–3]. Among them, polystyrene, poly-urethane, poly-ethylene, and elastomeric closed cell thermal insulation, which are made of organic substance, are mainly used as pipe insulation to prevent freezing and surface condensation by minimizing the heat loss [4–6]. However, pipe insulation could be ignited from the overheated hot wire or welding work for maintenance, and rapidly spread to the surrounding combustibles [7–9]. To fundamentally prevent the spread of fire occurred by pipe insulation, inorganic materials such as semi-combustible, which does not ignite at high temperature, is able to be applied. However, inorganic substance, especially molded stone wool, glass wool, etc., is not useful in the installation of piping compared to organic materials because of its highly absorbent feature as a mechanical weakness [10–12]. For these reasons, the specific material of pipe insulation is not regulated, and it is recommended to use materials that satisfy the fire retardants as an alternative [13]. The fire growth rate index (*FIGRA*) is a general method to evaluate the material in the fire-retardant performance in fire technology [14,15]. Therefore, the pipe insulation, which satisfies extremely low *FIGRA* values, should minimize the rapid spread of fire phenomenon even though the pipe insulation could not have the properties of the complete non-combustible.

However, the regulated test conditions, such as the compartment size, the thermal properties of the wall, and the ignition heat source, are not equal for each test standard [16–19]. It means that *FIGRA* for evaluating the flame-retardant performance of the pipe insulation depends on the test conditions. Thus, the thermal characteristics inside the compartment in accordance with test conditions are important to analyze a fire risk of the pipe insulation.

There are several studies that the fire-retardant performance test result is changed by the test conditions in the use of the same pipe insulation material. The temperature inside the compartment increases in proportion to the thermal ratio, as resulted in the study of H. Pretrel et al., analyzed by the correlation under the ventilated pool fire phenomenon by the thermal ratio of dimensionless variables including thermal conductivity coefficient, the thickness of the wall, and the opening area of the compartment [20].

The fire growth rate decreases as the ignition source decreases in the same volume of pipe insulation, since the time to reach the maximum heat release is decreased proportional to the delay time of ignition, as investigation of N. Hernandez with the predictive model of the phenomenon of the penetration of radiation to the solid materials [21]. In addition, the fire growth rate decreases in proportion to the size of volume space, in the research of R.R. Leisted et al. with the analyze of the temperature distribution by the time in the case of polyisocyanurate or stone wool in the 1/5 reduced scale compartment of ISO 13784-1 [22].

In accordance with the previous research, it can be predicted that *FIGRA* would not be equal for the same material due to the thermal conditions. However, to the authors' knowledge, there have been no research to predict *FIGRA* since the values of  $Q_{max}$  and  $t_{max}$  cannot be closed with previous investigations [20–24]. Especially, if the value of *FIGRA* for a highly combustible material is evaluated too low at a specified test condition, it can cause a risk for the material to be used for building construction. From this point of view, the quantitative analysis on *FIGRA* in accordance with the experiment conditions can be considered as a significant object in terms of the evaluation for the risk of fire spread. The object of this study aims to predict *FIGRA* of polyethylene foam pipe insulation in accordance with the scale factor ( $S_f$ ), the volume fraction of the pipe insulation ( $V_f$ ), and the ignition heat source ( $Q_{ig}$ ).

## 2. Materials and Methods

### 2.1. Heat Transfer Phenomenon

Figure 1 explains that the heat transmission phenomenon of a polyethylene foam pipe insulation in the semi-closed compartment space. As shown in this figure, the surface temperature of the pipe insulation increases to reach the reference temperature by the ignition heat source. Therefore, the mass loss of the pipe insulation can be quantified as [25,26].

$$\dot{m}_{f,r}''' = \rho A_0 Y_f^n Y_{O_2}^m e^{(-E/RT_r)} \quad (1)$$

where  $\dot{m}_{f,r}'''$ ,  $\rho$ ,  $A_0$ ,  $Y$ ,  $E$ ,  $R$ , and  $T_r$  are the mass loss rate per unit volume, the density of pipe insulation, the pre-exponential factor, the mass fraction, the activation energy (kJ/mole), the gas constant (8.314 kJ/kmole), and the reference temperature, respectively. The heat release rate during the vaporization of the combustible ( $Q_f$ ) can be expressed as,

$$Q_f = \eta \Delta h_c \dot{m}_{f,r}''' V_f \quad (2)$$

where  $\eta$ ,  $\Delta h_c$ , and  $V_f$  are the combustion efficiency, the heat of combustion, and the ignited insulation volume during the combustion time, respectively [27]. When the ignition of the pipe insulation takes place inside the compartment, the surface area, which reaches the reference temperature ( $T_r$ )

by convective heat from the free stream and the radiative heat from the flame and the wall, could be time-variant. Thus, the total heat release rate can be denoted as,

$$Q_t(t) = Q_f(t) + Q_{ig} \tag{3}$$

where  $t$  denotes the combustion time, and the total heat release rate ( $Q_t(t)$ ) and the heat release rate of the pipe insulation ( $Q_f(t)$ ) in Equation (3) should be a time-variant function due to  $A_f \rightarrow A_f(t)$ . However, the heat of combustion ( $\Delta h_c$ , kJ/kg), which is one of the thermochemical properties, has a constant value for the pipe insulation as shown in Equation (4) [28–30].

$$\Delta h_c = \frac{\int_{t=0}^{t=t_{final}} \dot{Q}_f(t) dt}{\eta \Delta m_f} = const \tag{4}$$

where  $\Delta m_f$  means that the mass loss after the combustion of the pipe insulation. The fire growth rate index (FIGRA) to classify the fire-retardant grade is defined as the ratio of the maximum heat release rate ( $Q_{max}$ ), which is the net heat of the pipe insulation, and the time ( $t_{max}$ ) to reach the maximum heat release rate ( $Q_{max}$ ) as denoted in Equation (5) [16].

$$FIGRA = \frac{Q_{max}}{t_{max}} \tag{5}$$

where FIGRA refers to a main parameter to evaluate the fire-retardant grade. As  $Q_{ig}$  increases,  $\dot{Q}_f(t)$  is varied in proportion, since the size of the solid surface to reach the reference temperature ( $T_r$ ) varies with the combustion time. However, when the heat of combustion ( $\Delta h_c$ ) in Equation (4) maintains a constant value with a fixed value of  $\Delta m_f$ , the integral value of  $Q_f(t)$  during the total combustion time should satisfy the first law of energy conservation. It means that  $Q_{max}$  increases as the total combustion time decreases, as shown in the lower right side in Figure 1. Especially, the convective and radiative heat can be mainly affected by the compartment space ( $V_M$ ), the volume of the combustibles ( $V_f$ ), and the geometrical shape of the opening area. Therefore, it is assumed that  $\dot{Q}_{max}$  and  $t_{max}$  can be functioned with the quantity of the volume of the compartment ( $V_M$ ), the volume of the combustibles ( $V_f$ ), and the ignition heat source ( $Q_{ig}$ ) as denoted in Equation (6).

$$Q_{max}, t_{max} \sim f(Q_{ig}, V_M, V_f) \tag{6}$$

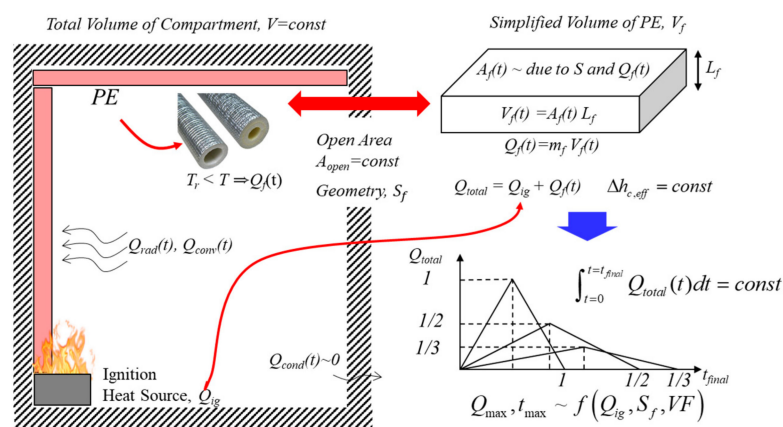


**Figure 1.** Schematic diagram of heat transfer and the heat release rate of the pipe insulation in a compartment fire.

### 2.2. Heat Transfer Phenomenon

Table 1 summarized the test conditions of ISO 20632 and NFPA 274. As shown in the table, the volume ( $V_M$ ) of the compartment was reduced to 1/3, 1/4, and 1/5 of ISO 20632. In addition, the volume fractions of the pipe insulation ( $VF$ ) consisted of a total 5 conditions, including those of ISO 20632 ( $VF = 0.024$ ) and NFPA 274 ( $VF = 0.07$ ). The experiment conditions of this study were opted with the definitions of the scale factor ( $S_f$ ) and the volume fraction ( $VF$ ) as denoted in Equation (6).

$$S_f = \frac{L_M}{L_{ISO}}, VF = \frac{V_f}{V_M} \tag{7}$$

where  $S_f$ ,  $V_M$ ,  $V_{ISO}$ ,  $V_f$ , and  $VF$  are the scale factor, the volume of the compartment, the volume of the ISO 20632 compartment, and the volume fraction of the pipe insulation, respectively. The schematic diagram and pictures of the experiment conditions are explained in Figure 2.

**Table 1.** Test conditions investigated by ISO 20632 and NFPA 274.

Contents	ISO 20632	NFPA 274	Test Conditions
Volume of Compartment (m <sup>3</sup> )	$V_{ISO} = 20.76 \text{ m}^3$	$V_{M,NFPA} = 0.78 \text{ m}^3$	$V_{M,1/3} = 0.768 \text{ m}^3$ $V_{M,1/4} = 0.324 \text{ m}^3$ $V_{M,1/5} = 0.165 \text{ m}^3$
Scale Factor (-)	1	1/3 (= 0.33)	1/3 (= 0.33), 1/4 (= 0.25), 1/5 (= 0.20)
Volume of Insulation (m <sup>3</sup> )	$V_{f,iso} = 0.51 \text{ m}^3$	$V_{f,NFPA} = 0.055 \text{ m}^3$	$V_{f,1/5} = 0.004 \text{ m}^3, 0.008 \text{ m}^3, 0.019 \text{ m}^3, 0.008 \text{ m}^3$ $V_{f,1/4} = 0.016 \text{ m}^3, 0.038 \text{ m}^3, 0.012 \text{ m}^3, 0.023 \text{ m}^3$ $V_{f,1/3} = 0.053 \text{ m}^3, 0.017 \text{ m}^3, 0.032 \text{ m}^3$
Volume Fraction (-)	$VF = 0.024$	$VF = 0.07$	$VF = 0.024, 0.05, 0.07, 0.1$
Ignition (kW) and Time (s)	$Q_{ig,1} = 100 \text{ kW for } 600 \text{ s}$ $Q_{ig,2} = 300 \text{ kW for } 600 \text{ s}$	$Q_{ig,1} = 20 \text{ kW for } 180 \text{ s}$ $Q_{ig,2} = 70 \text{ kW for } 420 \text{ s}$	$Q_{ig} = 10 \text{ kW}, 15 \text{ kW}, 20 \text{ kW for } t_{final} = 600 \text{ s}$

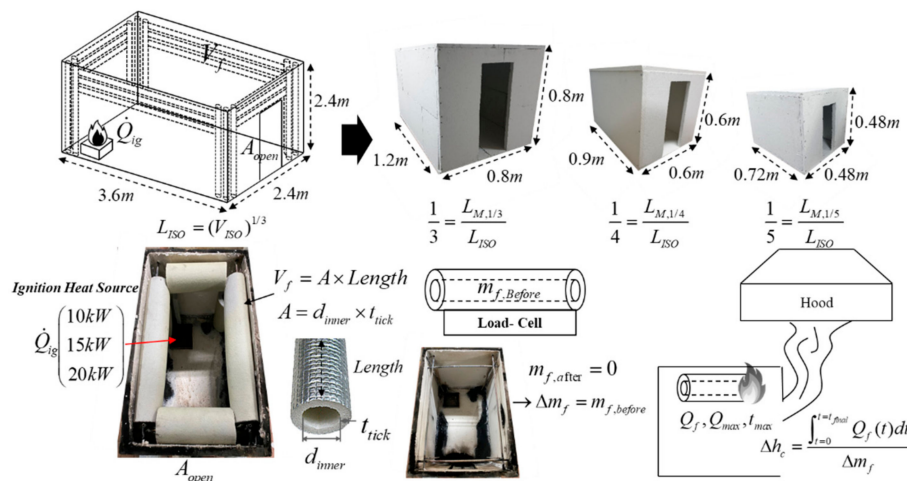


**Figure 2.** Schematic diagram and pictures of the test conditions and the experiment method.

### 2.3. Calibration of the Heat Release Rate

Figure 3 shows the calibration results of the heat release rate for a propane burner by the oxygen consumption method of the cone calorimeter. A mass flow controller (MFC, Model TSC-145) was used to control the flow rate of propane. In Figure 3a, the difference of maximum 50 s with the theoretical heat release rate was measured due to the increase of the response time of the MFC instrument. Thus, in the low flow range from 10 to 20 kW, the fluctuation of the mass flow rate and the delay time were minimized by the metering valve and the area flow meter. As a result of performing A-Type uncertainty under the repeated experiments, it is found that the cone-calorimeter apparatus used in this study had a reliability of  $\pm 5\%$  when the coverage factor,  $k = 1.95$  at 95% confidence level as displayed in Figure 3b. Table 2 shows the specifications of the experimental apparatus used in this study.

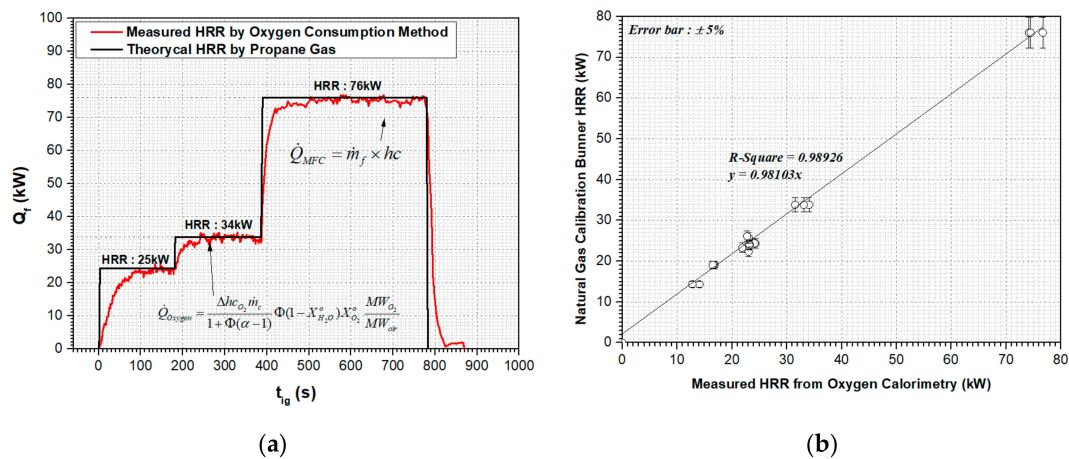


**Figure 3.** (a) Calibration results of heat release rate (HRR) using propane burner and (b) comparison of the theoretical and measured HRR.

**Table 2.** Specification of the experiment apparatus of the cone-calorimeter.

Measurement	Specification
Duct Temperature	K-Type Wire, Range: −200–1000 °C
DAQ	Voltage: 20 mV to 100 V, 1–5 V F.S., 20 channels, Accuracy: ±0.1%
Duct Size & Blower	Length: 5 m, Diameter: 0.2 m, Fan capacity: 3 hp
O <sub>2</sub> Analyzer	Output: 4–20 mA, Range: 0.7–1.2 bar, Model: OXYMAT 61
Pressure Sensor	Output: 0–10 V, Range: 1250 Pa, Model: MS-311
Mass Flow Controller	Fuel: CH <sub>4</sub> , C <sub>3</sub> H <sub>8</sub> , Output: 0–5 VDC, Range: 200 LPM, Model: TSC-145
Pressure Transmitter	Output: 0–20 mA, Range: 0–20 bar, Model: PSC-E-B-A-P-G

2.4. Material Properties of the Test Sample

Figure 4a shows the measurement of the mass loss rate of the standard specimen calcium oxalate to verify the accuracy of the apparatus of thermo gravimetric analysis (TGA, Model STA PT1000). The calcium oxalate changes in the symmetry of CaC<sub>2</sub>O<sub>4</sub>·H<sub>2</sub>O, CaC<sub>2</sub>O<sub>4</sub>, and CaCO<sub>3</sub> as mentioned in reference [31]. Thus, the reference temperature (T<sub>r</sub>) was given as 190 °C, 450 °C, and 700 °C at ±30 °C, and the mass reduction rate was measured as −12.99%, −19.15%, and −29.98%, respectively. The measured values were in good agreement within about ±0.6% to the reference values.

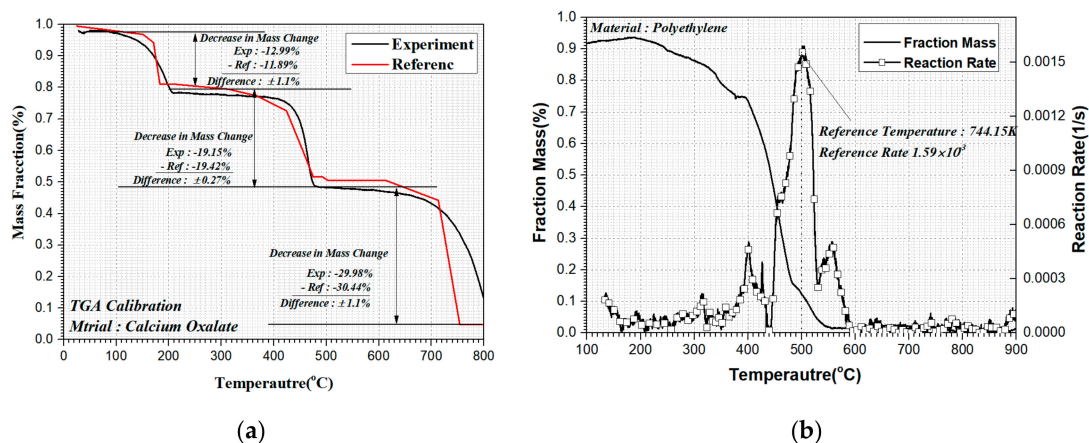


**Figure 4.** (a) Calibration results of TGA using calcium oxalate and (b) the results of TGA for material properties of the test sample (polyethylene foam).

Figure 4b shows the result of calculating the reaction rate, pre-exponential factor, and reference temperature, which are the thermochemical properties of the polyethylene foam pipe insulation used

in this study. The reaction and the heat rate mechanism of a solid fuel can be found in the combustion theory [32]. From  $T_r = 744$  K, the pre-exponential factor ( $A_j$ ) of Equation (8) and activation energy ( $E_j$ ) of Equation (9), which are suggested by Lyon et al. [30,33], are arranged in Table 3.

$$A_j = \frac{er_{p,j}}{Y_{s,0}} e^{\left(\frac{E_j}{RT_{p,j}}\right)} \quad (8)$$

$$E_j = \frac{er_{p,j}}{Y_{s,0}} \frac{RT_{p,j}^2}{(dT/dt)} \quad (9)$$

where  $A_j$ ,  $E_j$ ,  $T_r$ , and  $Y_{s,0}$  means the pre-exponential factor, activation energy, reference temperature, and mass fraction, respectively [33].

**Table 3.** Thermal properties of the polyethylene foam (PE) test sample.

Properties	Values	Properties	Values
Reference Temperature, (K)	744	Heat of Combustion, (kJ/kg)	42,660
Activation Energy (kJ/kmole)	$1.19 \times 10^{-5}$	Density (kg/m <sup>3</sup> )	26
Pre-exponential Factor (1/s)	$1.05 \times 10^{-6}$	Specific Heat (kJ/kg-°C)	2.31

### 3. Results and Discussion

#### 3.1. Experiment of Heat Release Rate

The effects of the ignition heat source on the heat release rate in the case of the fixed values of the scale factor ( $S_f = 1/3$ ) and the volume fraction ( $VF = 0.024$ ) are plotted in Figure 5. As denoted in this figure, the values of  $t_{max}$  were decreased as 589 s, 203 s, and 136 s in accordance with  $Q_{ig} = 12$  kW, 16 kW, and 23 kW, respectively. While  $Q_{max}$  maintained a constant value at approximately  $209 \pm 10$  kW. The results explained that the time for the pipe insulation to reach the reference temperature ( $T_r$ ) of 744 K decreased as  $Q_{ig}$  increased. However, the values of  $Q_{max}$  maintained a constant value since the overall heat amount of the pipe insulation inside the compartment should be conserved. All results for  $S_f = 1/3, 1/4, \text{ and } 1/5$  and  $VF = 0.024, 0.05, 0.07, \text{ and } 0.1$  in accordance with the ignition heat sources are plotted in Figure 6. Test conditions and analysis based on the Figure 6 are summarized in Table 4. As shown in Table 4,  $t_{max}$  of Test #8, #16, and #31–#33, which have more than 20% deviation, were excluded due to the environment differences. However, in all the experimental result, the values of  $Q_{max}$  maintained a constant value within the range of  $\pm 3.48\%$  average and  $\pm 12.26\%$  maximum for the fixed volume fraction ( $VF$ ), while the values of  $t_{max}$  were decreased, which were inversely proportional to the heat amount of ignition. From the results of Figure 6 and Table 4, the effective heat of combustion was investigated and  $Q_{max}$  and  $t_{max}$  were predicted with the effects of  $S_f$ ,  $VF$ , and  $Q_{ig}$ .

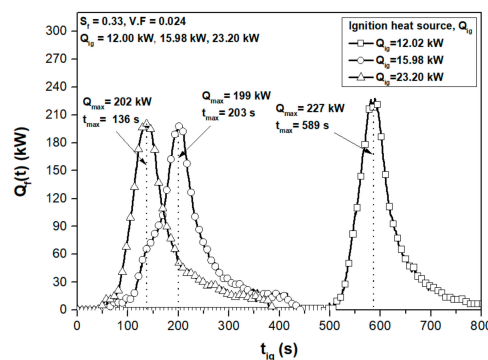


**Figure 5.** The results of the heat release rate with the variations of the ignition heat source for volume fraction 0.024 and scale factor 0.33.

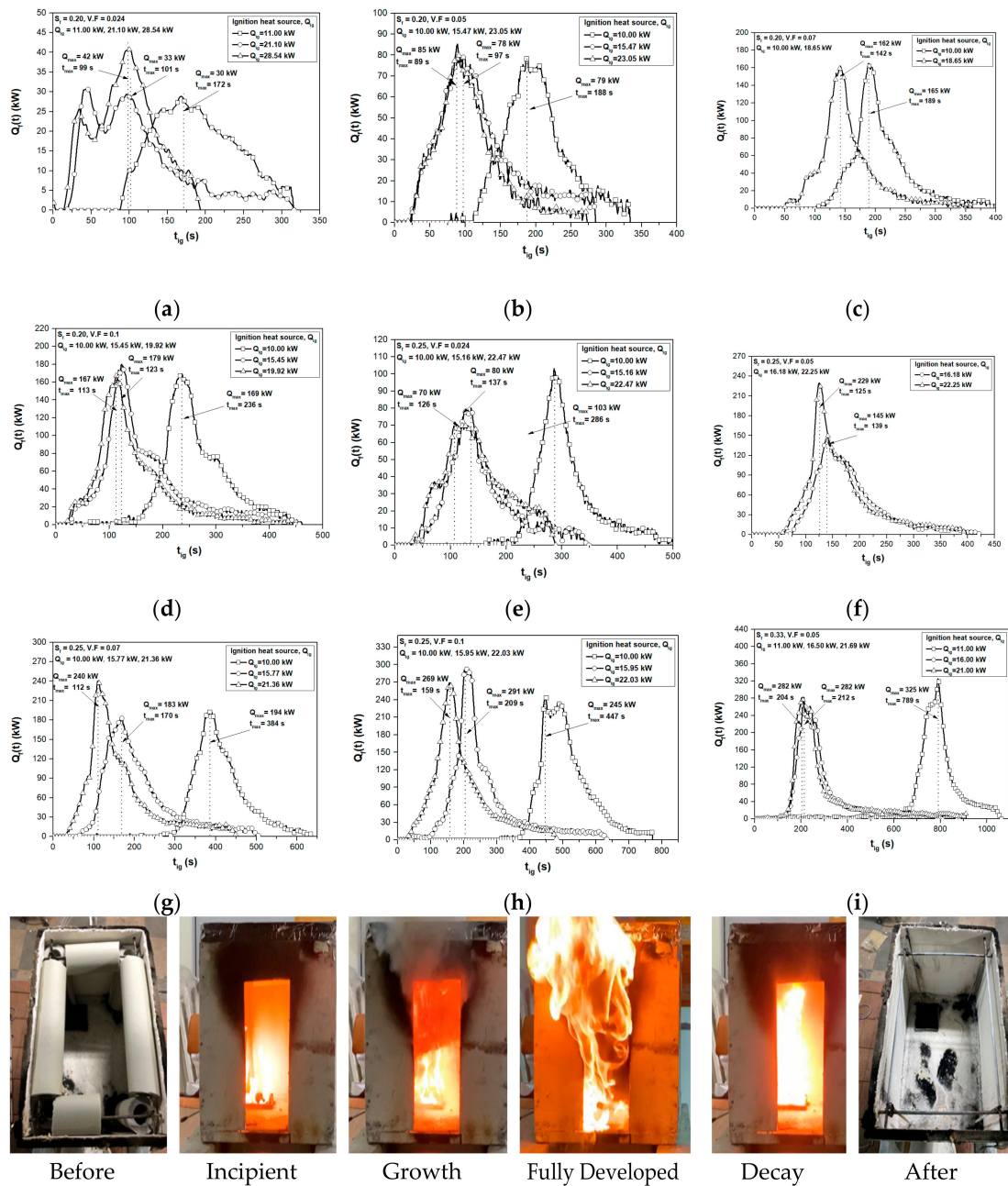


**Figure 6.** Experiment results of the heat release rate vs. ignition heat source for 0.33, 0.25, and 0.2 of the scale factor with a volume fraction of 0.024, 0.05, 0.07, and 0.1. (a) Test#1–Test#3. Heat release rate vs. time ( $S_f = 0.2, VF = 0.024, Q_{ig} = 11.00$  kW, 21.10 kW, 28.54 kW); (b) Test#4–Test#6. Heat release rate vs. time ( $S_f = 0.2, VF = 0.05, Q_{ig} = 10.00$  kW, 15.47 kW, 23.05 kW); (c) Test#7, Test#9. Heat release rate vs. time ( $S_f = 0.2, VF = 0.07, Q_{ig} = 10.00$  kW, 18.65 kW); (d) Test#10–Test#12. Heat release rate vs. time ( $S_f = 0.2, VF = 0.1, Q_{ig} = 10.00$  kW, 15.45 kW, 19.92 kW); (e) Test#13–Test#15. Heat release rate vs. time ( $S_f = 0.25, VF = 0.024, Q_{ig} = 10.00$  kW, 15.16 kW, 22.47 kW); (f) Test#17–Test#18. Heat release rate vs. time ( $S_f = 0.25, VF = 0.05, Q_{ig} = 16.18$  kW, 22.25 kW); (g) Test#19–Test#21. Heat release rate vs. time ( $S_f = 0.25, VF = 0.07, Q_{ig} = 10.00$  kW, 15.77 kW, 21.36 kW); (h) Test#22–Test#24. Heat release rate vs. time ( $S_f = 0.25, VF = 0.1, Q_{ig} = 10.00$  kW, 15.95 kW, 22.03 kW); and (i) Test#28–Test#30. Heat release rate vs. time ( $S_f = 0.33, VF = 0.05, Q_{ig} = 11.00$  kW, 16.50 kW, 21.69 kW).

**Table 4.** Test conditions and summarized results of experiments.

Test Num.	Test Conditions					Results of Experiment				
	$S_f$	$V_M$	$V_f$	$VF$	$\Delta m_f$	$\dot{Q}_{ig}$	$\dot{Q}_f$	$\Delta m_{c,eff}$	$\dot{Q}_{max}$	$t_{max}$
	(-)	(m <sup>3</sup> )	(m <sup>3</sup> )	(-)	(kg)	(kW)	(kJ)	(kJ/kg)	(kW)	(s)
#1	0.2	0.165	0.004	0.024	0.109	11.00	3795	34,817	30.23	172
#2	0.2	0.165	0.004	0.024	0.109	21.10	3797	34,833	33.47	101
#3	0.2	0.165	0.004	0.024	0.109	28.54	3779	34,672	42.63	99
#4	0.2	0.165	0.008	0.050	0.227	10.00	7477	32,938	79.09	188
#5	0.2	0.165	0.008	0.050	0.227	15.47	8576	37,778	78.96	97
#6	0.2	0.165	0.008	0.050	0.227	23.05	6913	30,455	85.23	89
#7	0.2	0.165	0.012	0.070	0.312	10.00	11,847	37,972	165.25	189
#8	0.2	0.165	0.012	0.070	0.320	14.64	10,785	33,702	160.78	N/A
#9	0.2	0.165	0.012	0.070	0.318	18.65	11,282	35,479	162.03	142
#10	0.2	0.165	0.0165	0.1	0.450	10.00	17,344	38,541	169.34	236
#11	0.2	0.165	0.0165	0.1	0.454	15.45	18,482	40,708	179.98	123
#12	0.2	0.165	0.0165	0.1	0.452	19.92	16,436	36,362	167.22	113
#13	0.25	0.324	0.008	0.024	0.223	10.00	8260	37,042	103.18	286
#14	0.25	0.324	0.008	0.024	0.214	15.16	7660	35,797	80.16	137
#15	0.25	0.324	0.008	0.024	0.220	22.47	9101	41,366	70.60	126
#16	0.25	0.324	0.016	0.050	0.444	10.00	18,959	42,699	178.05	N/A
#17	0.25	0.324	0.016	0.050	0.444	16.18	14,961	33,696	145.56	139
#18	0.25	0.324	0.016	0.050	0.444	22.25	17,763	40,006	229.68	125
#19	0.25	0.324	0.023	0.070	0.626	10.00	22,223	35,500	194.57	384
#20	0.25	0.324	0.023	0.070	0.632	15.77	23,994	37,964	183.09	170
#21	0.25	0.324	0.023	0.070	0.620	21.36	24,962	40,261	240.65	112
#22	0.25	0.324	0.032	0.1	0.892	10.00	35,515	39,815	245.92	447
#23	0.25	0.324	0.032	0.1	0.892	15.95	32,812	36,785	291.99	209
#24	0.25	0.324	0.032	0.1	0.872	22.03	33,095	37,953	269.13	159
#25	0.33	0.768	0.019	0.024	0.495	12.00	19,455	39,303	227.52	589
#26	0.33	0.768	0.019	0.024	0.500	15.98	20,547	41,095	199.78	203
#27	0.33	0.768	0.019	0.024	0.503	23.20	18,974	37,722	202.00	136
#28	0.33	0.768	0.038	0.050	1.052	11.00	44,035	41,859	325.05	789
#29	0.33	0.768	0.038	0.050	1.046	16.50	37,700	36,042	282.23	212
#30	0.33	0.768	0.038	0.050	1.054	21.69	39,344	37,328	282.02	204
#31	0.33	0.768	0.053	0.070	1.448	13.57	49,677	34,307	382.10	N/A
#32	0.33	0.768	0.053	0.070	1.430	17.69	54,897	38,389	437.19	N/A
#33	0.33	0.768	0.053	0.070	1.451	21.83	50,609	34,878	370.69	N/A

### 3.2. Comparison of the Effective Heat of Combustion, $\Delta h_{c,eff}$

Regarding the previous studies, the heat of combustion ( $\Delta h_c$ ) of the polyethylene foam pipe insulation is around 42,660 kJ/g [34]. In this study, the effective heat of combustion of Equation (10) as referred in [35] was compared with the heat of combustion by integrals on the combustion time under the measured heat release rate.

$$h_{c,eff} = \int_{t=0}^{t=t_{final}} Q_f(t) dt / \Delta m_f \quad (10)$$

where  $\Delta h_{c,eff}$  and  $\Delta m_f$  are the effective heat of combustion and the mass loss of the pipe insulation after combustion, respectively. The measured effective heat of combustion for  $S_f = 1/3, 1/4,$  and  $1/5, VF = 0.024, 0.05, 0.07,$  and  $0.1$  in accordance with the values of  $Q_{ig}$  are plotted in Figure 7. As shown in the figure, the average values of the effective heat of combustion was around 37,214 kJ/kg, which was only about 87% of the combustion efficiency compared to 42,660 kJ/kg. The main reason can be found that the incomplete combustion condition occurs due to the circumstance lack of ventilation regarding to the size of the opening area [34–37]. In addition, from R. N. Walters et al. [34], the combustion heat value could be changed by the composition ratio and the porosity of the molecule consisted

of materials. Therefore, the correlation between the geometric shape of the pipe insulation and the thermochemical properties of the molecular structure of the pipe insulation should be analyzed with the combustion efficiency to obtain more accuracy reasons. However, the main purpose of this study was to predict the fire growth rate index related with the scale factor ( $S_f$ ), the volume fraction ( $VF$ ), and the ignition heat source ( $Q_{ig}$ ). Therefore,  $Q_{max}$  and  $t_{max}$  were analyzed with the effective heat of combustion assumed to be the averaged value of 37,214 kJ/kg.

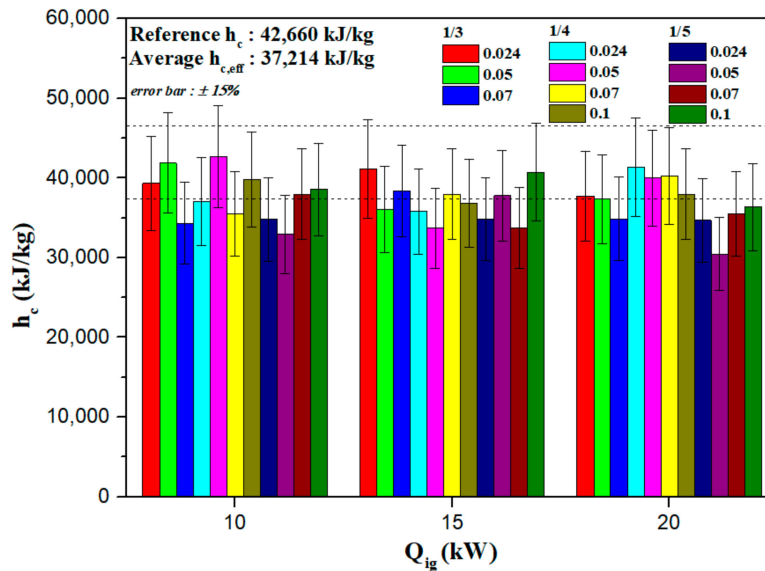


Figure 7. The results of the effective heat of combustions with volume fraction 0.024, 0.05, 0.07, and 0.1 for scale factor 1/3, 1/4, and 1/5.

### 3.3. Analysis of the Maximum Heat Release Rate, $Q_{max}$

The values of  $Q_{max}$  and  $\Delta m_f$  for  $S_f = 1/3, 1/4,$  and  $1/5$  and  $VF = 0.024, 0.05, 0.07,$  and  $0.1$  in Table 4 are plotted in Figure 8. The line marked in red can be obtain from the boundary condition, which is  $Q_{max} = 0$  at  $\Delta m_f = 0$ , as shown in the Equation (11).

$$Q_{max} = a_1 \times \Delta m_f^{b_1} \tag{11}$$

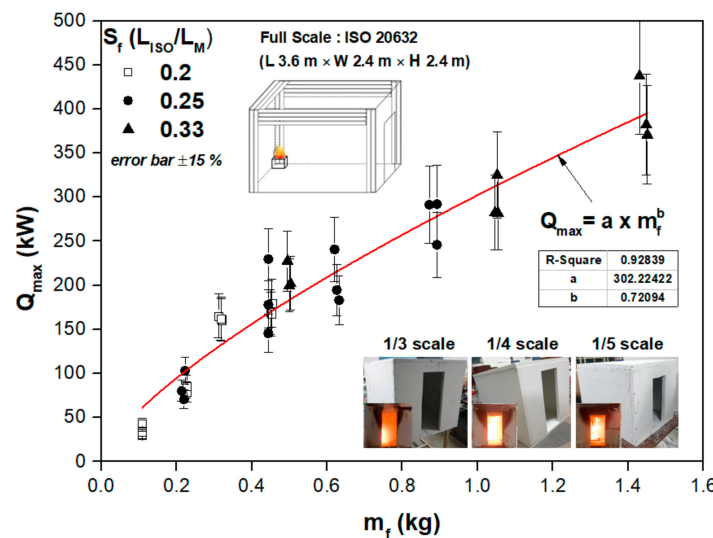


Figure 8. Experiment results of the maximum heat release rate vs. fuel mass loss with scale factors ( $S_f = 1/3, 1/4,$  and  $1/5$ ) and volume fraction ( $VF = 0.024, 0.05, 0.07,$  and  $0.1$ ).

The  $\Delta m_f$  can be assumed that the initial mass of the pipe insulation since all completely burned during the experiments for each condition in Table 4. The simple expression foam of  $Q_{max}$  can be curve-fitted with  $\Delta m_f$ , regardless of  $S_f$ ,  $VF$ , and  $Q_{ig}$  in the case of  $a_1 = 302.224$  and  $b_1 = 0.721$  within  $\pm 15\%$ . However, in the overall range of  $\Delta m_f$ , the deviations between Equation (11) and the experiments were higher in accordance with the volume of compartment and the pipe insulation. Thus, the effects of  $S_f$  and  $VF$  on  $Q_{max}$  were investigated to obtain more accurate prediction.

Figure 9a shows the correlations between  $Q_{max}$  and  $VF$  for  $S_f = 1/3, 1/4,$  and  $1/5$ . As shown in the figure,  $Q_{max}$  intends to increase in proportional to  $VF$  as denoted in Equation (12).

$$Q_{max,pre} = a_2(VF)^{b_2} \tag{12}$$

where  $Q_{max,pre}$  (kW),  $a_2$ (kW), and  $b_2$  are the predictive value of the maximum heat release rate and the experimental constants, respectively. The mass loss is approximated in Equation (13).

$$\Delta m_f = VF \times V_M \times \rho_f \tag{13}$$

when  $a_2$  is constant at 1766.78 of Equation (12),  $b_2$  decreases with  $S_f$  as shown in Figure 9b. Thus, the experiment constant,  $b_2$  can be curve-fitted as,

$$b_2 = 0.18308 \times S_f^{-1.04545} \tag{14}$$

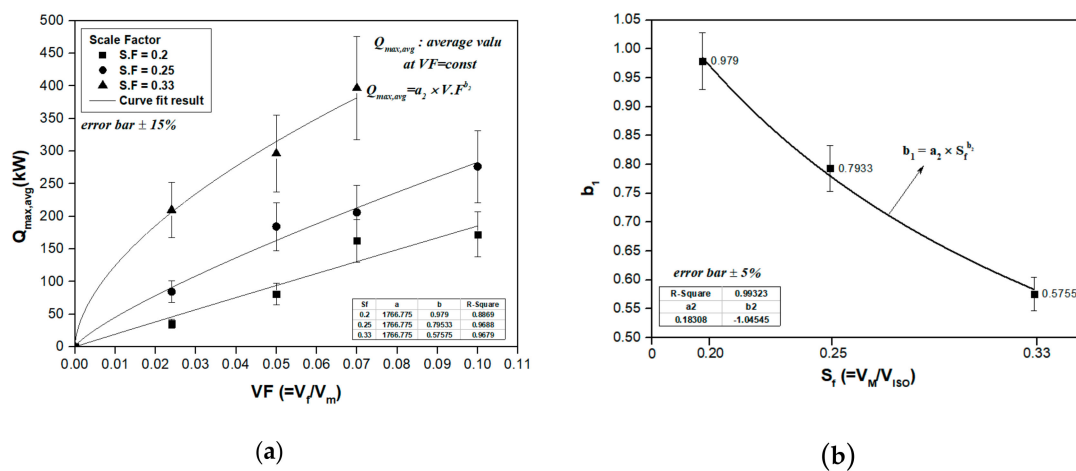


**Figure 9.** (a) Averaged maximum HRR vs. volume fraction for  $S_f = 0.2, 0.25,$  and  $0.33$  and (b) the curve-fit results of experiment coefficient  $b_1$  vs. scale factor for  $S_f = 0.2, 0.25,$  and  $0.33$ .

The predictions of  $Q_{max}$  and  $\Delta m_f$  for the fixed values of the scale factor ( $S_f = 1/3, 1/4,$  and  $1/5$ ) and the volume fraction ( $VF = 0.024, 0.05, 0.07,$  and  $0.1$ ) were compared with the experiments as shown in Figure 10. The predictions at  $\Delta m_f = 0.2$  kg and  $0.7$  kg were higher about 15% than the experiments for Test #14, #15, and #18 in Table 4 due to the relatively high deviation of the averaged  $Q_{max}$ . On the other hand, the predictions at  $\Delta m_f = 0.2$  kg were about 15% lower than the experiments for Test#7 and #9 in Table 4. The main reason would be expected to take place from the combustion efficiency in accordance with the opening area [20]. However, it is confirmed that the total of 27 experiments and the predicted values were in good agreement within  $\pm 5\%$ . Thus, Equation (12) indicates that the improved accuracy approximately 10% or more compared to Equation (11) since  $S_f$  and  $VF$  were considered. The limitation of the prediction should consider the experiment constants. The prediction of  $Q_{max}$  can be applicable in the case of establishing the database of various types of insulation.

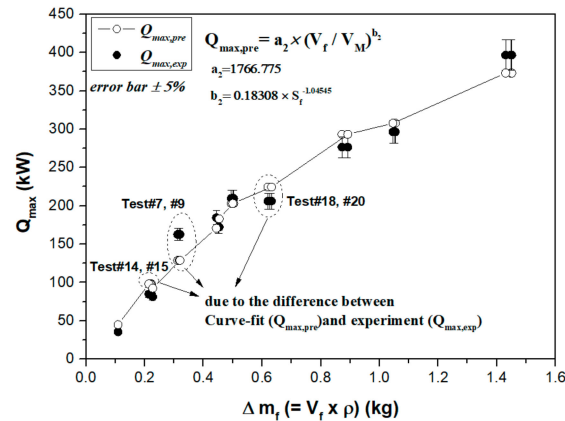


Figure 10. Comparison of the maximum heat release rate of experiments and predictions with mass loss.

3.4. Analysis of the Time to Reach the Maximum Heat Release Rate,  $t_{max}$

From the results in Table 2, as the volume of the compartment increased, the heating time of the surface temperature for the pipe insulation by convection and radiation was proportionally increased in the case of the fixed values of  $Q_{ig}$  and  $VF$ . In addition, when  $Q_{ig}$  increased,  $t_{max}$  was decreased since the surface area of the pipe insulation to reach reference temperature ( $T_r$ ) rapidly increased. These relations can be functioned as,

$$t_{max} \sim f(S_f / Q_{ig}) \tag{15}$$

Figure 11a shows the relations between  $S_f / Q_{ig}$  and  $t_{max}$  in the case of  $VF = 0.024, 0.05, 0.07,$  and  $0.1$ . The values of  $t_{max}$ , which was inversely proportional to  $Q_{ig}$  and proportional to  $S_f$  under the fixed value of  $VF$ , can be curve-fitted as,

$$t_{max,pre} = c_1 + c_2 \times e^{(c_3 \times S_f / Q_{ig})} \tag{16}$$

where  $c_1, c_2,$  and  $c_3$  represent the experimental constants for the polyethylene foam pipe insulation. The values of  $c_2$  and  $c_3$  were found to have the constant with 3.283 and 180.102. In addition, the values of the experimental constant  $c_1$  were 74.93, 81.07, 83.35, and 122.64 when  $VF = 0.024, 0.05, 0.07,$  and  $0.1$  respectively, as shown in Figure 11b. Thus, it can be curve fitted as,

$$c_1 = d_1 + d_2 \times e^{(d_3 \times VF)} \tag{17}$$

where  $d_1, d_2,$  and  $d_3$  have a constant value of 75.782, 0.167, and 56.36, respectively.

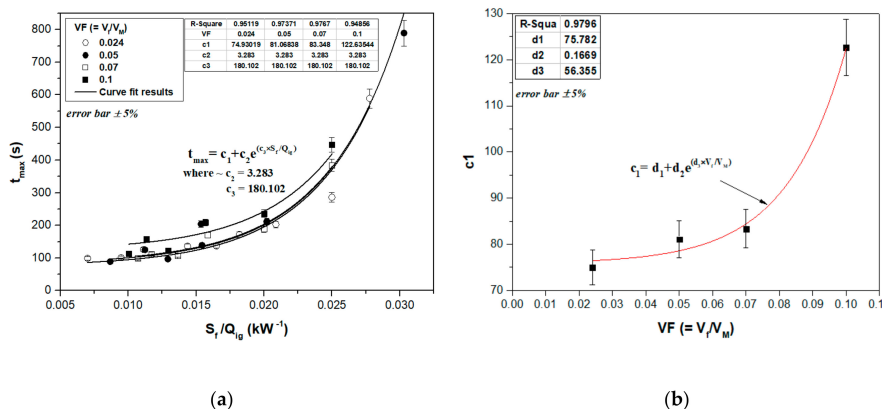


Figure 11. (a) Maximum time vs.  $S_f / Q_{ig}$  for 0.024, 0.05, 0.07, and 0.1 of the volume fraction and (b) the curve-fit results of experiment coefficient  $c_1$  vs. volume Fraction.

The predictions of  $t_{max}$  and  $S_f/Q_{ig}$  for the fixed values of the scale factor ( $S_f = 1/3, 1/4,$  and  $1/5$ ) and the volume fraction ( $VF = 0.024, 0.05, 0.07,$  and  $0.1$ ) were compared with the experiments as shown in Figure 12. The predictions at  $S_f/Q_{ig} = 0.01, 0.015,$  and  $0.024 \text{ kW}^{-1}$  were about 20% deviation than the experiments for Test #5, #6, #11, #12, #13, #15, and #30 in Table 4 due to the heat loss by the leakage from the connection part in the compartment, the difference humidity or the relatively low surrounding temperature. The heat loss can cause the experiments of  $t_{max}$  that could be relatively delayed than the predictions of  $t_{max}$ . However, the total 23 of predictions were in good agreement with the experiments in the error range of  $\pm 5\%$ . Therefore, as mentioned in Section 3.3,  $t_{max}$  can be applicable in the case of establishing the database of various types of insulation. As denoted in Equations (12) and (16), the predictions of  $Q_{max}$  and  $t_{max}$  were significantly correlated with  $S_f, VF,$  and  $Q_{ig}$ , which were the test conditions of fire resistance standard. It is noticeable that the values of FIGRA can be obtained without experiments for the polyethylene foam pipe insulation if the effects of the thermal properties of the compartment materials are determined.

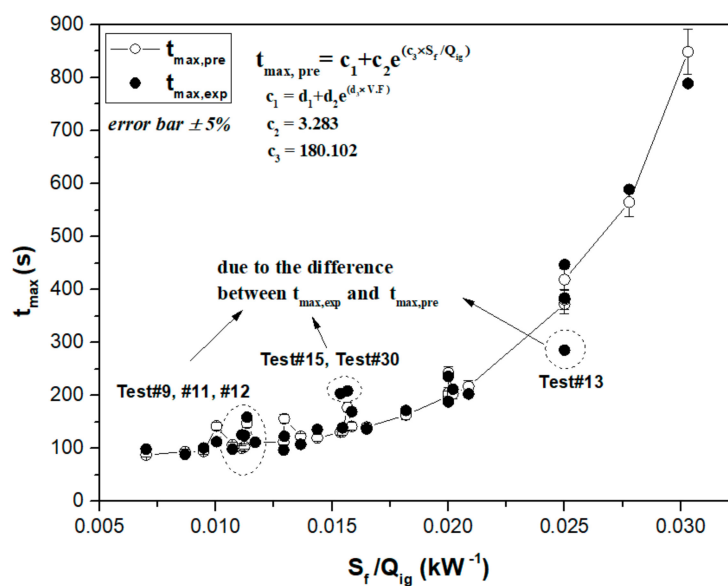


Figure 12. Comparison of the maximum time of experiments and predictions with  $S_f/Q_{ig}$ .

### 3.5. Estimation of the Fire Growth Rate Index, FIGRA

According to EN13501-1, the fire-retardant grade can be divided as Grade A<sub>2</sub> for  $FIGRA \leq 0.16$  kW/s, Grade B for  $0.16 \leq FIGRA \leq 0.6$  kW/s, Grade C for  $0.6 \leq FIGRA \leq 1.5$  kW/s, the Grade D for  $0.6 \leq FIGRA \leq 7.5$  kW/s, and Grade E for  $FIGRA \geq 7.5$  kW/s. Therefore, Equations (12) and (16) are substituted into Equation (5), and the prediction of FIGRA can be arranged as,

$$FIGRA_{pre} = \frac{a_2(VF)^{b_2}}{c_1 + c_2 \times e^{(c_3 \times S_f / Q_{ig})}} \tag{18}$$

where  $FIGRA_{pre}$  means the prediction value of the fire growth rate index (FIGRA) considering the scale factor ( $S_f$ ), the volume ratio ( $VF$ ), and the ignition heat source ( $Q_{ig}$ ).

Figure 13 shows the results of the comparisons between the predictions by Equation (18) and the experiments in Table 4. The predictions of  $Q_{max}$  for Test #15, #20, and #30 in Table 4 were about 11% higher than the experiments, while the predictions of  $t_{max}$  were about 16% lower than the experiments at  $FIGRA = 0.975 \text{ kW/s}, 1.58 \text{ kW/s},$  and  $2.40 \text{ kW/s}$ . On the other hand, the predictions of  $Q_{max}$  for Test #7 and #8 in Table 4 were about 19% lower than the experiments, while the predictions of  $t_{max}$  were about 10% lower than the experiments at  $FIGRA = 0.63 \text{ kW/s}$  and  $1.05 \text{ kW/s}$ . These results caused more than a 30% deviation of  $FIGRA_{pre}$  and  $FIGRA$ . It would be necessary to investigate the

combustion efficiency and the surrounding temperature with environmental conditions to improve more accurate predictions. However, the final results shows that a total of 22 of the predictions were in good agreement with the experiments within  $\pm 15\%$  since the predicted values of  $Q_{max}$  and  $t_{max}$  were satisfied with the experiments on the effects of  $S_f$ ,  $VF$ , and  $Q_{ig}$  within  $\pm 5\%$ . Especially, in the case of application of FIGRA of EN 13501-1, the polyethylene foam pipe insulation could have Grade B, C, or D in accordance with  $S_f$ ,  $VF$ , and  $Q_{ig}$ .

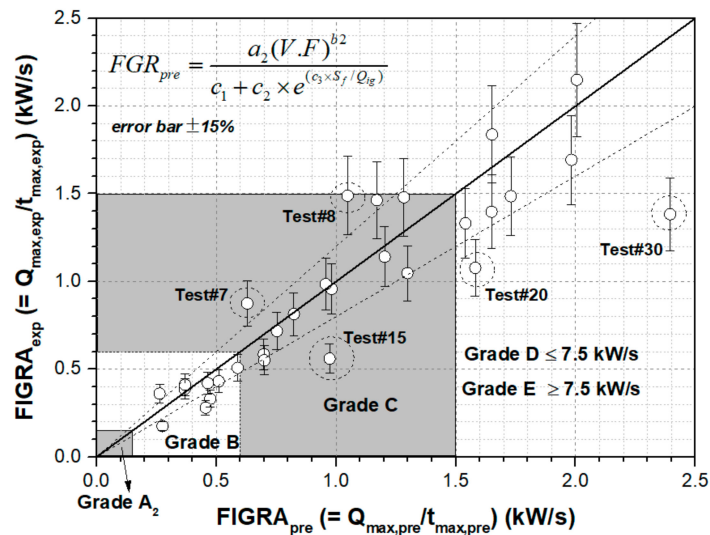


**Figure 13.** The comparison of the predictions and experiment of the fire growth rate index with scale factors ( $S_f = 1/3, 1/4, \text{ and } 1/5$ ), volume fraction ( $VF = 0.024, 0.05, 0.07, \text{ and } 0.1$ ), and ignition heat sources ( $Q_{ig}$ ).

#### 4. Conclusions

In this study, the effects of the scale factor ( $S_f$ ), the volume fraction ( $VF$ ), and the ignition heat source ( $Q_{ig}$ ) on the fire growth rate index ( $FIGRA$ ) of polyethylene foam pipe insulation were systematically investigated. From the 33 experiments of the heat release rate of the pipe insulation, the maximum heat release rate ( $Q_{max}$ ), and the time ( $t_{max}$ ) to reach the maximum heat release rate were analyzed with the effective heat of combustion assumed to be the averaged value of 37,214 kJ/kg. The results of this study can be summarized as follows,

First, the values of  $Q_{max}$  maintained a constant value within the range of  $\pm 3.48\%$  average and  $\pm 12.26\%$  maximum regardless of  $Q_{ig}$  when the value of  $VF$  was fixed. While  $t_{max}$  decreased, which was inversely proportional to  $Q_{ig}$ . These results explain that the heat amount of the pipe insulation should be conserved regardless of the ignition.

Second, the correlations between the values of  $Q_{max}$  and  $t_{max}$  in accordance with the variation of the scale factor ( $S_f = 1/3, 1/4, \text{ and } 1/5$ ), the volume fraction ( $VF = 0.024, 0.05, 0.07, \text{ and } 0.1$ ), and the ignition heat source ( $Q_{ig} = 10 \text{ kW}, 15 \text{ kW}, \text{ and } 20 \text{ kW}$ ) were presented. It is possible to quantify that  $Q_{max}$  intended to increase in proportional to  $VF$  and  $S_f$  regardless of  $Q_{ig}$  while  $t_{max}$  increased in proportion to  $S_f/Q_{ig}$  and  $VF$ . However, the limitation of the predictions was that the experiment coefficients should be determined with the thermal properties of the wall and the type of the pipe insulation.

Finally,  $FIGRA$  as defined in EN 13501-1 was evaluated using the prediction models of the  $Q_{max}$  and  $t_{max}$ . It was verified that a total of 22 experiments in Table 4 were in good agreement with the predictive values of  $FIGRA$  within  $\pm 15\%$ . Especially, the fire-retardant grade for the polyethylene foam pipe insulation could have a Grade B, C, and D in accordance with the scale factor ( $S_f = 1/3, 1/4, \text{ and } 1/5$ ), volume fraction ( $VF = 0.024, 0.05, 0.07, \text{ and } 0.1$ ), and the ignition heat sources ( $Q_{ig}$ ). Therefore, in case of establishing the database of various types of insulation, it can be expected that the prediction models could apply to evaluate the fire-retardant performance with dimensionless methods for  $FIGRA$ .

**Author Contributions:** Conceptualization, J.W.P., O.K.L. and W.J.Y.; methodology, W.J.Y.; software, J.W.P.; validation, J.W.P. and W.J.Y.; formal analysis, W.J.Y.; investigation, J.W.P., O.K.L.; resources, W.J.Y.; data curation, W.J.Y.; writing—original draft preparation, W.J.Y.; writing—review and editing, W.J.Y.; visualization, J.W.P.; supervision, J.W.P., O.K.L.; project administration, W.J.Y.; funding acquisition, W.J.Y. Please turn to the CRediT taxonomy for the term explanation. Authorship must be limited to those who have contributed substantially to the work reported. All authors have read and agreed to the published version of the manuscript.

**Funding:** This research was supported by the Field-oriented Support of Fire Fighting Technology Research and Development Program funded by the Ministry of Public Safety and Security (2018-NFA002-008-01020000-2019).

**Acknowledgments:** This research was funded by the National Fire Agency (Republic of Korea), grant number 2018-NFA002-008-01020000-2019.

**Conflicts of Interest:** The authors declare no conflict of interest. The funders had no role in the design of the study; in the collection, analyses, or interpretation of data; in the writing of the manuscript, or in the decision to publish the results.

## References

1. Kecebas, A. Determination of insulation thickness by means of exergy analysis in pipe insulation. *Energy Convers. Manag.* **2012**, *58*, 76–83. [[CrossRef](#)]
2. Kayfeci, M.; Yabanova, I.; Kecebas, A. The use of artificial neural network to evaluate insulation thickness and life cycle costs: Pipe insulation application. *Appl. Therm. Eng.* **2014**, *63*, 370–378. [[CrossRef](#)]
3. Kecebas, A.; Alkan, M.A.; Bayhan, M. Thermo-economic analysis of pipe insulation for district heating piping systems. *Appl. Therm. Eng.* **2011**, *31*, 17–18. [[CrossRef](#)]
4. Mangs, S. *Insulation Materials in District Heating Pipes: Environmental and Thermal Performance of Polyethylene Terephthalate and Polyurethane Foam*; Chalmers University of technology: Göteborg, Sweden, 2005; pp. 1–2.
5. Vega, A.; Yarahmadi, N.; Jakubowicz, I. Determination of the long-term performance of district heating pipes through accelerated ageing. *Polym. Degrad. Stab.* **2018**, *153*, 15–22. [[CrossRef](#)]
6. Winkler-Skalna, A.; Łoboda, B. Determination of the thermal insulation properties of cylindrical PUR foam products throughout the entire life cycle using accelerated aging procedures. *J. Build. Eng.* **2020**, *31*, 101348. [[CrossRef](#)]
7. Hilado, C.J.; Cumming, H.J. Fire Safety Aspects of Thermal Insulation. *J. Therm. Insul.* **1977**, *1*, 116–128. [[CrossRef](#)]
8. Goldfarb, I.; Zinoviev, A. A study of delayed spontaneous insulation fires. *Phys. Lett. A* **2003**, *311*, 491–500. [[CrossRef](#)]
9. Hidalgo, J.P.; Welch, S.; Torero, J.L. Performance criteria for the fire safe use of thermal insulation in buildings. *Constr. Build. Mater.* **2015**, *100*, 285–297. [[CrossRef](#)]
10. Ye, L.; Meng, X.Y.; Ji, X.; Li, Z.M.; Tang, J.H. Synthesis and characterization of expandable graphite–poly (methyl methacrylate) composite particles and their application to flame retardation of rigid polyurethane foams. *Polym. Degrad. Stab.* **2009**, *94*, 971–979. [[CrossRef](#)]
11. Xu, W.; Chen, R.; Du, Y.; Wang, G. Design water-soluble phenolic/zeolitic imidazolate framework-67 flame retardant coating via layer-by-layer assembly technology: Enhanced flame retardancy and smoke suppression of flexible polyurethane foam. *Polym. Degrad. Stab.* **2020**, *176*, 109152. [[CrossRef](#)]
12. D'Alessandro, F.; Baldinelli, G.; Sambuco, S.; Rufini, A. Experimental assessment of the water content influence on thermo-acoustic performance of building insulation materials. *Constr. Build. Mater.* **2018**, *158*, 264–274. [[CrossRef](#)]
13. Sundström, B. *The Development of a European Fire Classification System for Building Products*; Department of Fire Safety Engineering, Lund University: Lund, Sweden, 2007.
14. European Committee for Standardization. *EN ISO 11925-2 Reaction to Fire Tests—Ignitability of Building Products Subjected to Direct Impingement of Flame—Part 2: Single-Flame Source Test*; European Committee for Standardization: Brussels, Belgium, 2010.
15. European Committee for Standardization. *EN ISO 13823 Reaction to Fire Tests—Building Products—building Products Excluding Floorings Exposed to the Thermal Attack by a Single Burning Item*; European Committee for Standardization: Brussels, Belgium, 2002.

16. European Committee for Standardization. *EN ISO 13501-1 Reaction to Fire Tests—Fire Classification of Construction Products and Building Elements-Part 1: Classification using Test Data*; European Committee for Standardization: Brussels, Belgium, 2002.
17. NFPA. *NFPA Standard 274: Standard Test Method to Evaluate Fire Performance Characteristics of Pipe Insulation*; Technical Report; National Fire Protection Association: Quincy, MA, USA, 2013.
18. European Committee for Standardization. *EN ISO 13501-1 Reaction to Fire Tests—Small Room Test for Pipe Insulation Products or Systems*; European Committee for Standardization: Brussels, Belgium, 2008.
19. Janssens, M.L.; Huczek, J.; Saucedo, A. Development of a model of the ASTM E 84 Steiner tunnel test. *Fire Saf. Sci.* **2008**, *9*, 279–289. [[CrossRef](#)]
20. Pretrel, H.; Bouaza, L.; Suard, S. Multi-scale analysis of the under-ventilated combustion regime for the case of a fire event in a confined and mechanically ventilated compartment. *Fire Saf. J.* **2020**, *5*, 103069. [[CrossRef](#)]
21. Hernández, N.; Fuentes, A.; Reszka, P.; Fernández-Pello, A.C. Piloted ignition delay times on optically thin PMMA cylinders. *Proc. Combust. Inst.* **2019**, *37*, 3993–4000. [[CrossRef](#)]
22. Leisted, R.R.; Sørensen, M.X.; Jomaas, G. Experimental study on the influence of different thermal insulation materials on the fire dynamics in a reduced-scale enclosure. *Fire Saf. J.* **2017**, *93*, 114–125. [[CrossRef](#)]
23. You, W.J.; Park, J.W.; Sin, J.Y.; Park, H.G.; Ohk, K.L. Analysis of the Maximum Heat Release Rate in Accordance with the Test Method of the Flame Retardant Performance for Pipe Insulation. *Fire Sci. Eng.* **2020**, *34*, 18–25. [[CrossRef](#)]
24. Ohk, K.L.; Nam, D.G.; Jang, H.Y. Evaluation of the Reaction-to-fire Performance of Pipe Insulation Material using Small Room Test. *Fire Sci. Eng.* **2019**, *33*, 1–8.
25. McGrattan, K.; Klein, B.; Hostikka, S.; Floyd, J. *Fire Dynamics Simulator (Version 5), User's Guide*; NIST Special Publication; NIST: Gaithersburg, MD, USA, 2010; pp. 56–57.
26. Quintiere, J.G. *Fundamentals of Fire Phenomena*; John Wiley & Sons: West Sussex, UK, 2006; pp. 96–133.
27. Tewarson, A.; Jiang, F.H.; Morikawa, T. Ventilation controlled combustion of polymers. *Combust. Flame* **1993**, *95*, 151–169. [[CrossRef](#)]
28. Madrigal, J.; Guijarro, M.; Hernando, C.; Diez, C.; Marino, E. Effective heat of combustion for flaming combustion of Mediterranean forest fuels. *Fire Technol.* **2011**, *47*, 461–474. [[CrossRef](#)]
29. Al-Ghouti, M.; Al-Degs, Y.; Mustafa, F. Determination of hydrogen content, gross heat of combustion, and net heat of combustion of diesel fuel using FTIR spectroscopy and multivariate calibration. *Fuel* **2010**, *89*, 193–201. [[CrossRef](#)]
30. Lyon, R.E.; Walters, R.N. Pyrolysis combustion flow calorimetry. *Anal. Appl. Pyrolysis* **2004**, *71*, 27–46. [[CrossRef](#)]
31. Minakshi, M.; Visbal, H.; Mitchell, D.R.; Fichtner, M. Bio-waste chicken eggshells to store energy. *Dalton Trans.* **2018**, *47*, 16828–16834. [[CrossRef](#)] [[PubMed](#)]
32. Minakshi, M.; Barmi, M.; Mitchell, D.R.; Barlow, A.J.; Fichtner, M. Effect of oxidizer in the synthesis of NiO anchored nanostructure nickel molybdate for sodium-ion battery. *Mater. Today Energy* **2018**, *10*, 1–14. [[CrossRef](#)]
33. Lyon, R.E. An integral method of nonisothermal kinetic analysis. *Thermochim. Acta* **1997**, *297*, 117–124. [[CrossRef](#)]
34. Walters, R.N.; Hackett, S.M.; Lyon, R.E. Heats of combustion of high temperature polymers. *Fire Mater.* **2000**, *24*, 245–252. [[CrossRef](#)]
35. Bundy, M.F.; Hamins, A.P.; Johnsson, E.L.; Kim, S.C.; Ko, G.; Lenhart, D.B. *Measurements of Heat and Combustion Products in Reduced-Scale Ventilation-Limited Compartment Fires*; Technical Note (NIST TN) -1483; National Institute of Standards and Technology: Gaithersburg, MD, USA, 2007; pp. 114–116.
36. Van Krevelen, D.W. Some basic aspects of flame resistance of polymeric materials. *Polymer* **1975**, *16*, 615–620. [[CrossRef](#)]
37. Filipczak, R.; Crowley, S.; Lyon, R.E. Heat release rate measurements of thin samples in the OSU apparatus and the cone calorimeter. *Fire Saf. J.* **2005**, *40*, 628–645. [[CrossRef](#)]

